Fast neutron detection with pressurized ^{4}He scintillation detectors

2012 JINST 7 C03035

(http://iopscience.iop.org/1748-0221/7/03/C03035)

PUBLISHED BY IOP PUBLISHING FOR SISSA MEDIALAB

RECEIVED: *January 9, 2012*
ACCEPTED: *February 20, 2012*
PUBLISHED: *March 19, 2012*

2nd INTERNATIONAL WORKSHOP ON FAST NEUTRON DETECTORS AND APPLICATIONS,
NOVEMBER 6–11 2011,
EIN GEDI, ISRAEL

Fast neutron detection with pressurized ^{4}He scintillation detectors

R. Chandra,[a,1] **G. Davatz,**[a,b] **H. Friederich,**[a,b] **U. Gendotti**[a] **and D. Murer**[a,b]

[a]*Arktis Radiation Detectors Ltd,*
Technoparkstrasse 1, 8005 Zurich, Switzerland
[b]*ETH Zurich, Institute for Particle Physics,*
Schafmattstrasse 20, 8093 Zurich, Switzerland

E-mail: rico.chandra@arktis-detectors.com

ABSTRACT: Measurement result and performance parameters are presented for fast neutron detectors exploiting the scintillation of natural helium at high pressure. This detection medium has a very low electron density, minimizing the sensitivity to gamma radiation and thus enabling neutron detection also in high gamma radiation environment. Contrary to proportional counters, scintillation detection enables fast (nanosecond) timing and pulse shape discrimination, a technique that enables a lower neutron detection threshold. In this work, the basic principles of the detector are described, followed by a study of gamma rejection capabilities. Methods to calibrate the detector are discussed. Finally, a brief description of a ^{4}He scintillation based detector system including data acquisition electronics is given.

KEYWORDS: Scintillators, scintillation and light emission processes (solid, gas and liquid scintillators); Neutron detectors (cold, thermal, fast neutrons); Noble-liquid detectors (scintillation, ionization two-phase)

[1]Corresponding author.

doi:10.1088/1748-0221/7/03/C03035

Contents

1 Neutron detection with ^{4}He scintillation

1.1 Elastic scattering

It is worth introducing this neutron detection technology by comparing it to ^{3}He neutron detectors, the "gold standard" of neutron detection. Figure 1 compares the neutron capture cross-section of ^{3}He with the elastic scattering cross-section of ^{4}He (natural helium). ^{3}He has a high capture cross-section for low energy neutrons; for this reason it is used in conjunction with moderators to deliver high detection efficiency over large area. In comparison, the elastic scattering cross-section of ^{4}He is substantially smaller in the low energy region. Interestingly for fast neutron detection, this cross section exhibits a peak that is located at roughly 1 MeV, nicely matching the peak emission of fission neutrons.

In this work ^{4}He is used as a fast neutron detection medium, exploiting the relatively large elastic scattering cross section in the energy range of fission neutrons. In an elastic scattering interaction, energy is transferred from an incoming neutron to a ^{4}He nucleus. The neutron is not absorbed in the process. For kinematic reasons, the maximum energy transfer from an incoming neutron to a ^{4}He nucleus is 64% of the neutron's energy prior to the interaction.

Figure 2 shows a Geant4 Monte-Carlo [1, 2] generated plot of the efficiency as a function of incoming neutron energy for elastic scattering to take place. These values can be interpreted as the detector's intrinsic interaction efficiency, in the case of this work over an area of 125 cm^2 per detector. The term "interaction efficiency" has been used rather than "detection efficiency" because gamma rejection — indispensible for practical applications — reduces this efficiency to an extent depending on the required gamma rejection capability, and the particular method with which rejection is performed.

2012 JINST 7 C03035

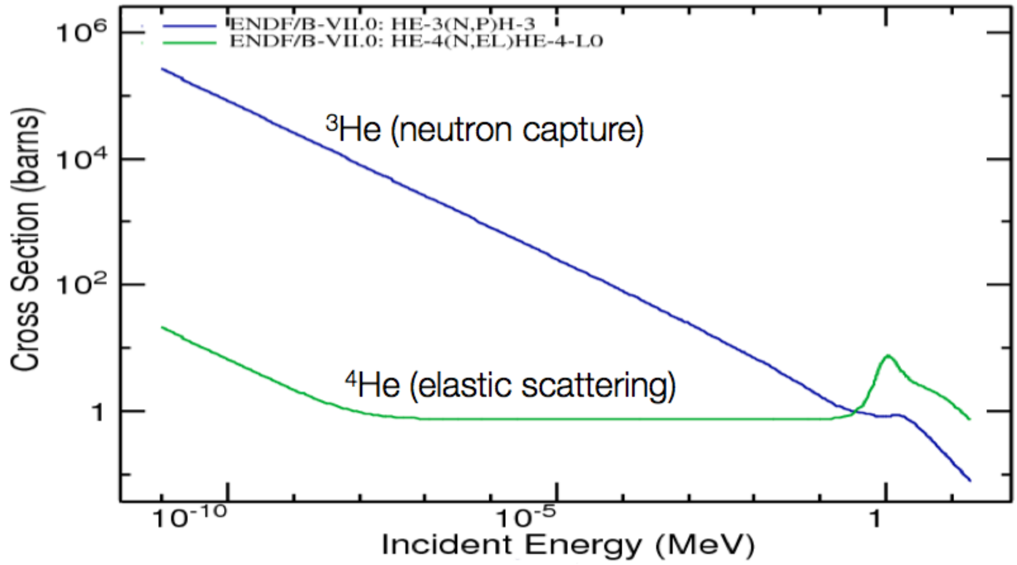

Figure 1. The elastic scattering cross-section of ^{4}He exhibits a peak at around 1 MeV, matching the emission spectrum of fission neutrons rather well [3].

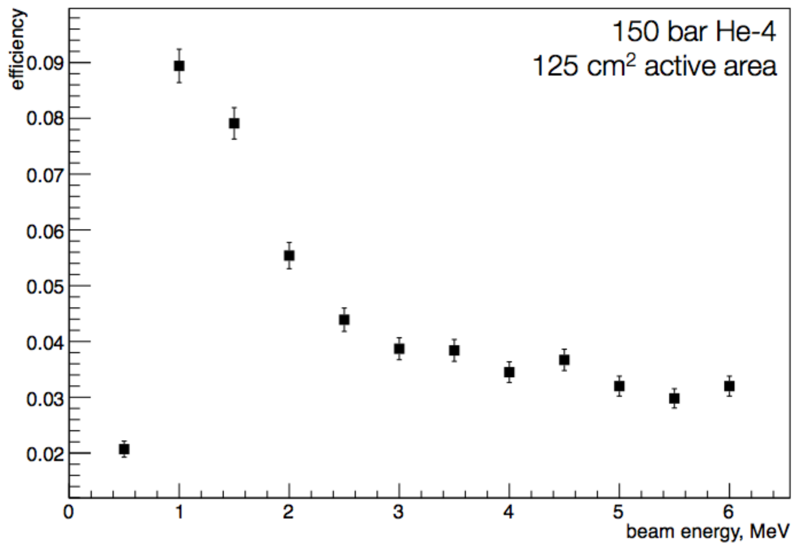

Figure 2. The interaction efficiency as a function of neutron energy over an active area of 125 cm^2 of the detectors used.

1.2 ^{4}He scintillation

^{4}He, like most noble gases, is a fairly good scintillator, with a light yield of the order of NaI crystals [7]. Noble gas scintillation light is in the vacuum ultraviolet (VUV) region requiring the use of a wavelength shifter in order to be detected in a meaningful way. ^{4}He scintillation light has a wavelength of the order of 70 nm. This work suggests that approximately 18 000 VUV photons are produced per MeV deposited by neutrons in 200 bar ^{4}He.

2012 JINST 7 C03035

1.3 Gamma rejection

With only two electrons per atom, ^{4}He has a very low charge density, thereby significantly limiting the sensitivity to gamma radiation. This is useful for fast neutron detection, where gamma rejection is often the single factor that limits performance the most.

In the case of ^{4}He scintillation detectors, there are four physical effects that contribute to gamma rejection performance:

1. Low gamma interaction probability. The low charge density of ^{4}He mentioned above severely reduces the probability of gamma interactions in the detector volume. The limit of this effect is attained when electrons ejected from the detector wall start playing a dominant role compared to interactions within the ^{4}He gas.

2. Low energy deposit. For the same reasons as above, the energy loss of recoiling Compton electrons in 200 bar ^{4}He gas is about 40 times lower than in a liquid scintillator. As such, a recoiling electron cannot deposit much energy in the gas before colliding with a detector wall.

3. Lower light yield for gammas. Unlike liquid scintillators where the light yield per deposited energy from gamma interactions is higher than for neutron interactions, the converse is believed to be the case in pressurized ^{4}He scintillation, due to inefficient recombination of electron-ion pairs.

4. Pulse shape discrimination. Like most noble gas, ^{4}He scintillation signals allow for powerful pulse shape discrimination, discussed below.

High-pressure ^{4}He scintillation signals exhibit a fast and a slow scintillation component, similar to liquid helium [8]. The former typically has a decay time of few nanoseconds, while the latter has a decay time of the order of one microsecond, see figure 3. These time constants are believed to be attributable to the singlet and triplet states of the excimers formed upon excitation of atomic ^{4}He; similar effects can be observed in other noble gases.

In the detectors used, depending on the type of interaction — gamma or neutron — the relative strengths of the two scintillation components are observed to be different, allowing their distinction. An example is shown in figure 3 (a) and (b). While the amplitude of the fast component is of the order of 120 mV for both signals (gamma and neutron), the number of photoelectrons detected in the slow component is approximately a factor 3–4 larger for the neutron event. The differentiation on the base of the fast versus slow component is often referred to as pulse shape discrimination.

Neutron interactions lead to ^{4}He recoils, where energy is deposited very locally within the gas. Gamma interactions lead to recoil electrons, which deposit only tens of keV's per centimeter of trajectory, as described above. This difference in energy density and therefore ionization density is believed to be what enables the pulse shape discrimination capability. Due to the large difference between the decay times of the two components, pulse shape discrimination properties are not affected by time spread effects introduced by the light collection.[1]

[1]Time spreads in the signals become larger with increasing detector size. This effect can lead to problems to perform pulse shape discrimination for liquid scintillators, due to the fact that the scintillation time constants do not differ substantially.

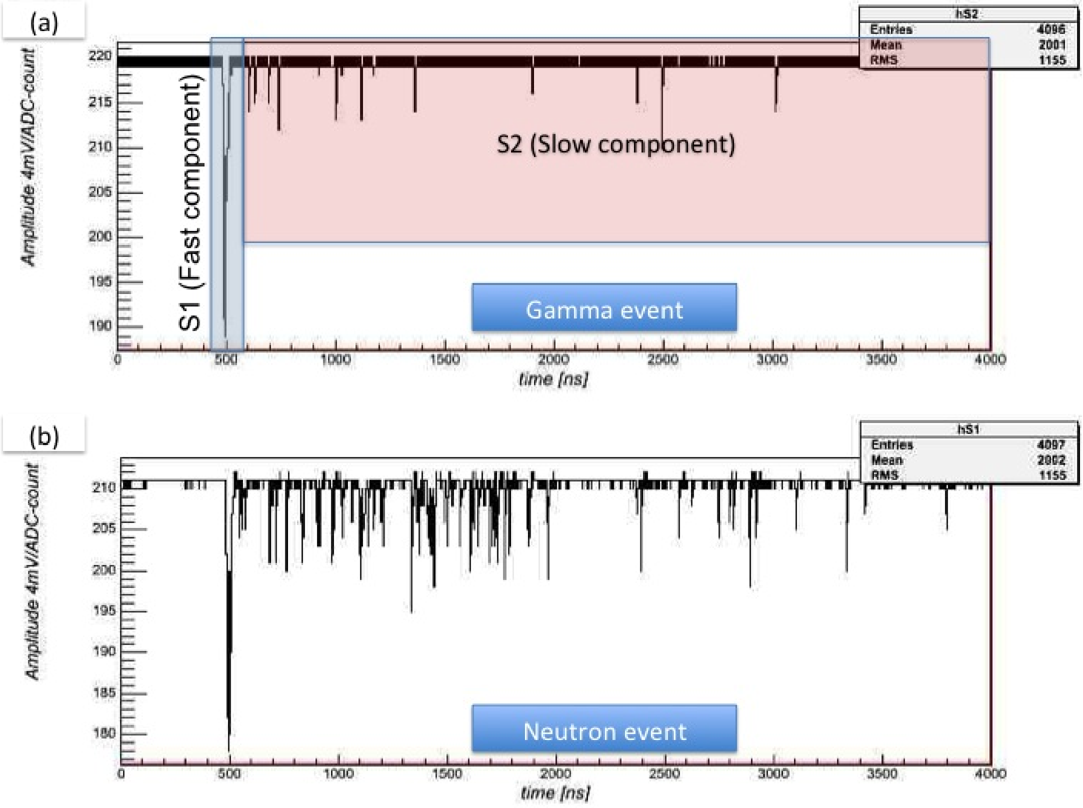

Figure 3. (a) ^{4}He scintillation signals consist of a fast component with a decay time of few nanoseconds and a slow component of the order of a microsecond. Depending on the type of interaction the relative strengths of the two scintillation components are observed to be different. (a) shows a gamma event. (b) shows a neutron event.

Figure 4 shows the difference in relative intensity of scintillation signals from neutron and gamma interactions. Red markers indicate measured signals from exposing the detector to a ^{60}Co gamma source. Black markers indicate measured signals from exposing the detector to an AmBe source, emitting both neutrons and high-energy gammas. Interestingly, the behavior observed is different than what would be expected from liquid argon scintillation measurements. In liquid argon scintillation, neutron signals have a higher ratio of fast to slow scintillation emission than gamma signals. The converse is observed in high-pressure helium. The curved shape of the neutron band in figure 4 is likely caused by nonlinearities in the data acquisition system of large signals. The curved shape is unlikely to be a caused by a wall-effect, as the range of recoiling alpha particles is short in high-pressure helium. The saturation effect of the electronics is reproducible with a pulse generator.

Discrimination between neutron and gamma events can be achieved by applying cuts to the parameters characterizing the relative intensities of the scintillation components. This work applies a threshold to the slow scintillation component, notionally depicted in figure 4 by the line labeled “lazy cut”. A comparison of the gamma/neutron discrimination using the slow scintillation component is shown in figure 5.

2012 JINST 7 C03035

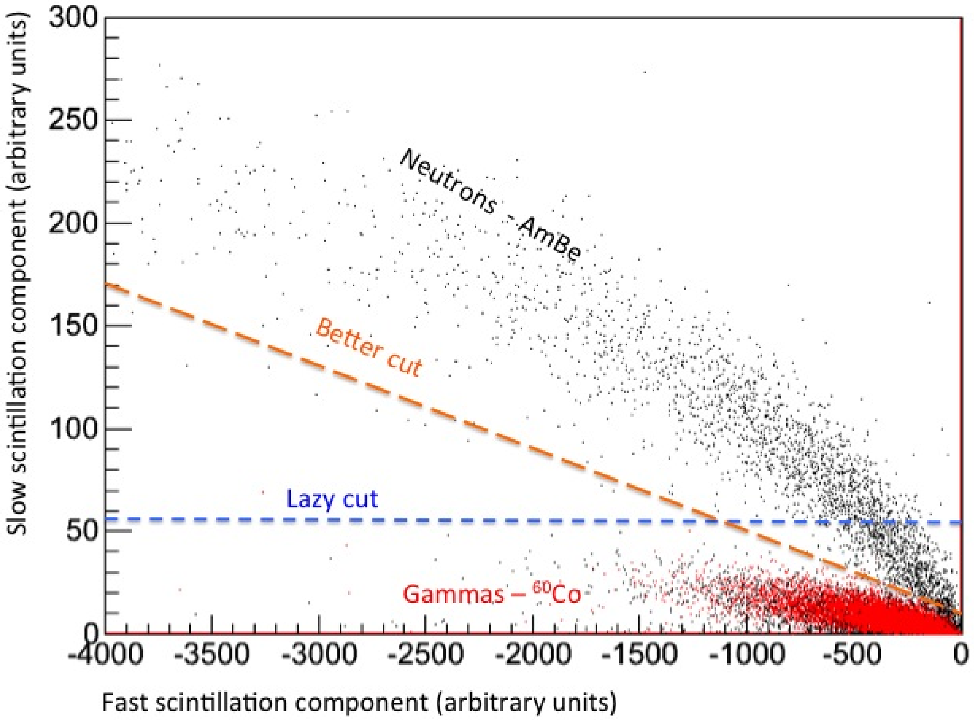

Figure 4. Scintillation signals from neutron interactions can be distinguished from gamma interactions on the basis of the larger ratio of photons in the slow scintillation component. The dotted lines notionally show the cuts described in the text.

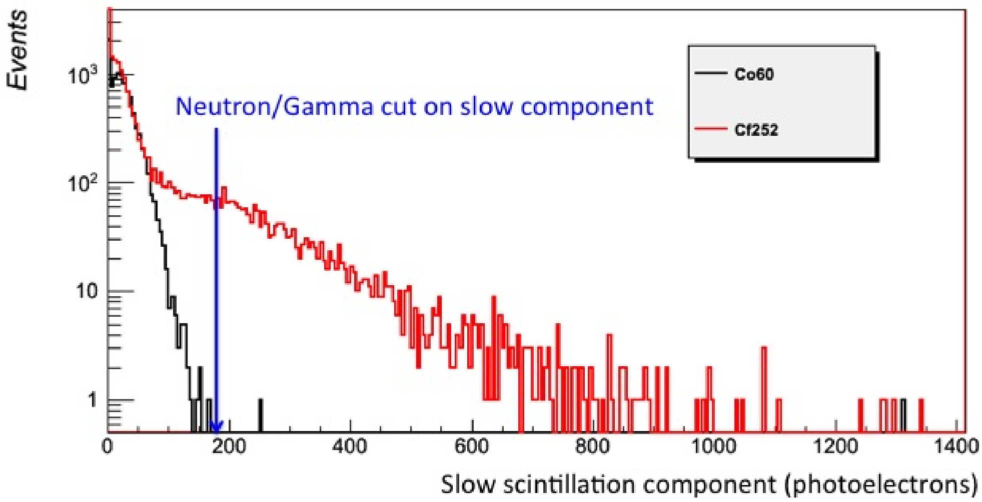

Figure 5. Histogram of the number of detected slow component photons from a ^{60}Co gamma source placed in contact with the detector (black entries) and a ^{252}Cf source (red entries). The "lazy cut" sacrifices neutron detection efficiency.

While being rather simple this cut sacrifices neutron detection efficiency in the region of interest when detecting fission neutrons. With this current cut, rejecting ^{60}Co dose rates of the order of 1 mSv/h to better than 0.03 counts per second, an intrinsic fission neutron detector efficiency of

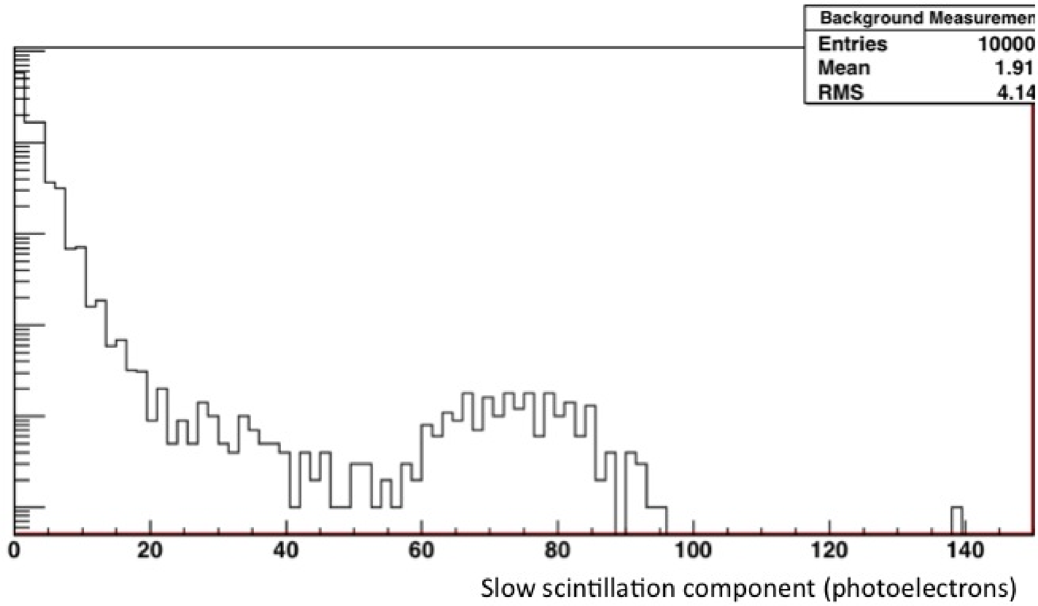

Figure 6. Histogram of the number of detected slow component photons taken in a 15 hour background run. A clear peak can be seen, attributed to the three alpha emission lines of the ^{222}Rn decay chain. This peak was used for energy calibration. This measurement was performed with 50% optical attenuation filters in place.

3% was measured. Substantial efficiency improvement for fission neutron detection is expected to be achievable through the use of a more sophisticated cut. The discrimination between neutron and gamma interactions is carried out in the digital domain.

1.4 Energy calibration and resolution

Accurately calibrating a ^{4}He scintillation detector is not a straightforward process, especially not if performing the calibration is expected to be a practical procedure. One way to achieve a relative calibration is to look at the cut-off of the energy deposition spectrum of gamma radiation in the detector. Figure 5 shows a histogram of the detected slow component of scintillation for a ^{60}Co gamma source placed on top of a detector. A clear cut-off can be made out. This calibration process is practical, but only gives a relative calibration.

A more practical and accurate way to perform the energy calibration was investigated. This method exploits trace quantities of ^{222}Rn, inadvertently introduced during the gas purification process. ^{222}Rn decays emit an alpha particle with a half-life of 3.8 days. This decay is followed by a chain of decays with substantially shorter half-life. Within relatively short time, three alpha decays take place, ^{222}Rn to ^{218}Po, ^{218}Po to ^{214}Pb, and ^{222}Po to ^{210}Pb, with defined alpha energies of 5.5, 6, and 7.7 MeV, respectively. The detector's natural background count rate is extremely low in this energy range. Therefore, long measurements ($>$ 12 hours and more) can be carried out to obtain a peak from these alpha decays, see figure 6. This peak can be used for calibration. The detector medium being ^{4}He, alpha particles have identical kinematics as nuclear recoils.

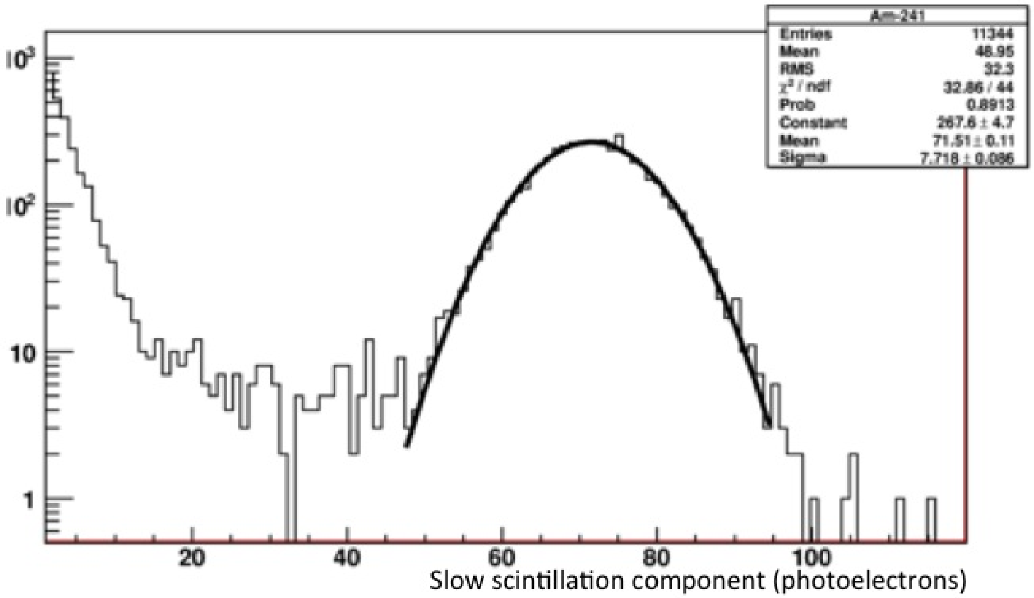

Figure 7. Histogram of the number of detected slow component photons in a measurement carried out with a 3 Bq Am-241 alpha source placed inside a detector. The peak width is compatible with the effect of photostatistics of approximately 10%. This measurement was performed with 50% optical attenuation filters in place.

The ^{222}Rn peak intensity was monitored over time. An exponential decay with a fair agreement with the expected 3.8 day half life was observed.

The detector's energy resolution was estimated by placing a 3 Bq ^{241}Am alpha source inside a detector, see figure 7. The width of the line is measured to have a width of approximately 10%, a value expected from photostatistics.

1.5 Timing and energy information

The timing and energy information of the ^{4}He detectors was studied using the Time of Flight (TOF) technique with an AmBe source. In this study two YAP crystals deliver a START signal. The YAP detectors are placed close to the source and detect the gamma rays produced in coincidence with the (α, n) reaction. The ^{4}He detector is placed at a distance of 60 and 90 cm from the source and is used to generate the STOP signal. The time difference between the gammas detected by the YAP crystals and the neutron detected by the ^{4}He detector defines the TOF of the neutron, see figure 8.

Figure 9 shows the TOF spectra acquired at two distances between the source and the detector. The prompt peak is produced when a neutron interacts with the YAP crystal and the gamma is detected by the ^{4}He detector, or by a gamma Compton scatter in the YAP. This peak defines the time $t = 0$ of the TOF spectrum. The peak observed at larger times is caused by neutrons. The change in the flight distance is clearly visible as a shift in the neutron TOF peak.

Another interesting aspect that shows the capability of ^{4}He scintillation detectors to measure timing and energy information of the detected neutron is the correlation between the TOF and the energy deposit. At a fixed distance between the detector and the source, increasing TOF corre-

2012 JINST 7 C03035

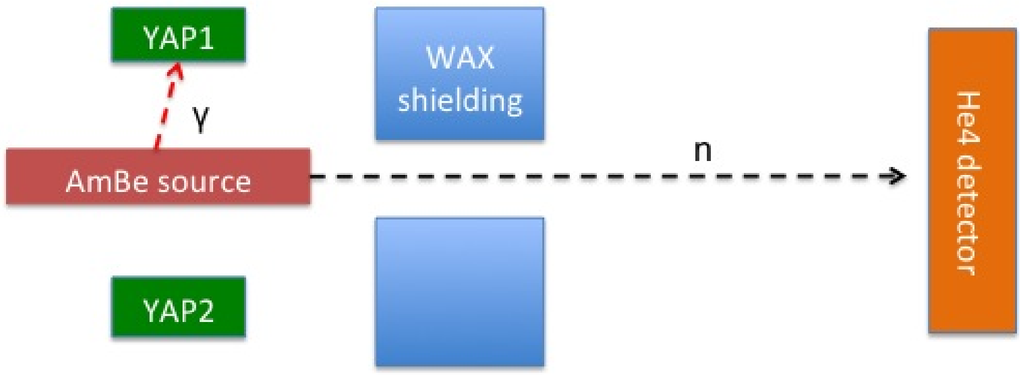

Figure 8. Schematic view of the set-up used for the TOF measurement.

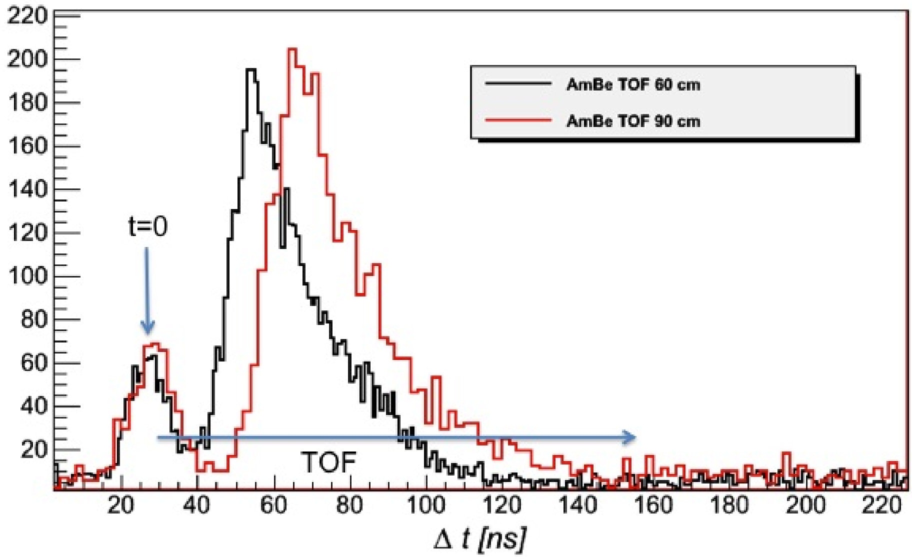

Figure 9. TOF spectra acquired at 60 and 90 cm distance between source and detector. The change in the distance is clearly visible as a shift in the TOF peak.

sponds to decreasing neutron energy. This effect is clearly visible in figure 10, where the TOF is plotted versus the number of photoelectrons detected in the slow scintillation component.

2 ^{4}He detector system

2.1 ^{4}He scintillation detectors

Figure 11 shows a schematic view of the detectors used. A cylindrical high-pressure vessel, sealed by windows at both ends, is read out by two photomultiplier tubes (PMTs). Due to the short wavelength of ^{4}He scintillation light, the walls of the detection volume are coated with a wavelength shifting material (WLS). A photo of such a detector module is given in figure 12.

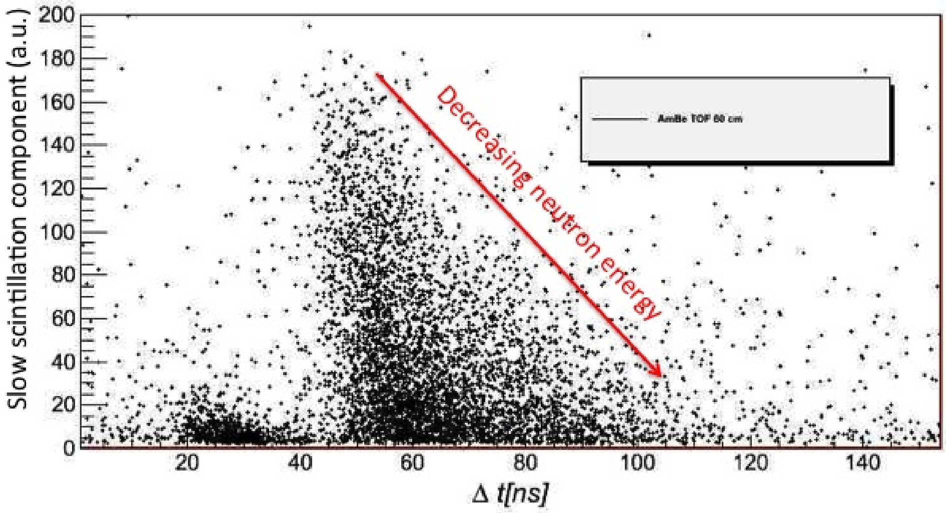

Figure 10. Correlation between the energy deposited in the detector and the TOF of the neutron. The increasing flight time is correlated with a decreasing energy deposit.

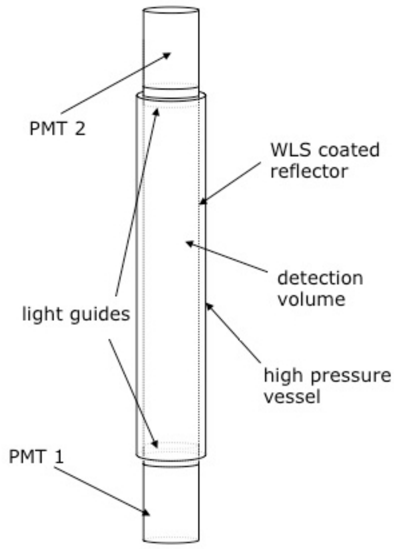

Figure 11. A schematic drawing of the ^{4}He scintillation detectors used.

2.2 Data acquisition electronics

The PMT signals are digitized by bespoke data acquisition cards [3], see figure 13. A field programmable gate array (FPGA) searches for coincidences in the signals of PMTs mounted on each detector. When such a coincidence indicating a particle interaction is found, the FPGA reads out a switched capacitor array [6] with the stored waveform. In this manner, excellent time resolution (1 Gs/s sampling and nanosecond time stamping even between different detectors) can be achieved at 10-bit resolution.

2012 JINST 7 C03035

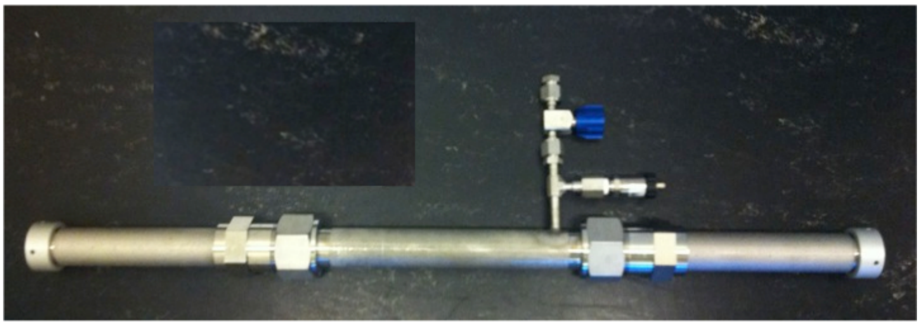

Figure 12. A photo of a ^{4}He scintillation detector used.

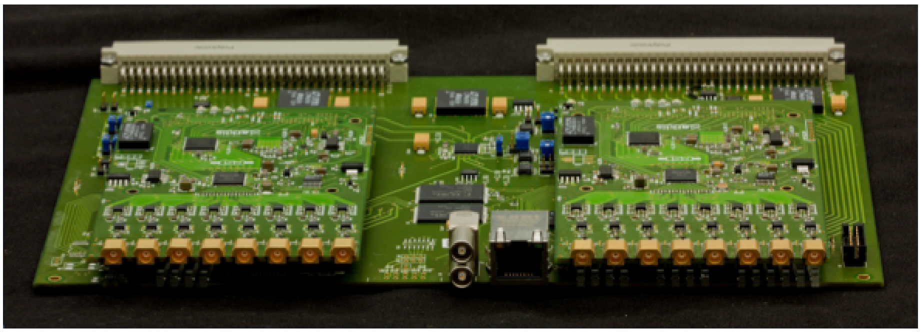

Figure 13. A photo of the data acquisition electronics used to digitize the signals with 10 bit resolution, 1 GS/s sampling rate, and nanosecond time stamps over all channels. This board can digitize 16 channels, further boards can be linked together, maintaining nanosecond time stamps across all boards.

All further analysis, including pulse shape discrimination, is carried out in the digital domain. Time resolutions of 2.2 nanoseconds have been achieved, a value that is dominated by the PMT's electron transit time differences. By virtue of the two-sided readout, events can be localized along the detector axis with a position resolution of approximately 10 cm.

2.3 System

Using the components described above, modular detection systems consisting of 2, 4, and 8 detectors were tested. Figure 14 shows the ENSFA system of 4 detectors, used for plutonium content measurements in mixed oxide (MOX) nuclear reactor fuel [4]. Future plans foresee a scaling up of such detection systems to 32 and 64 detectors for the passive detection of special nuclear materials. Fast neutron detectors are inherently scalable, as they do not suffer under self-shadowing effects the same way as thermal neutron detectors. Furthermore, the described detectors do not rely on any rare or expensive materials such as ^{3}He, making them attractive for large scale applications.

2012 JINST 7 C03035

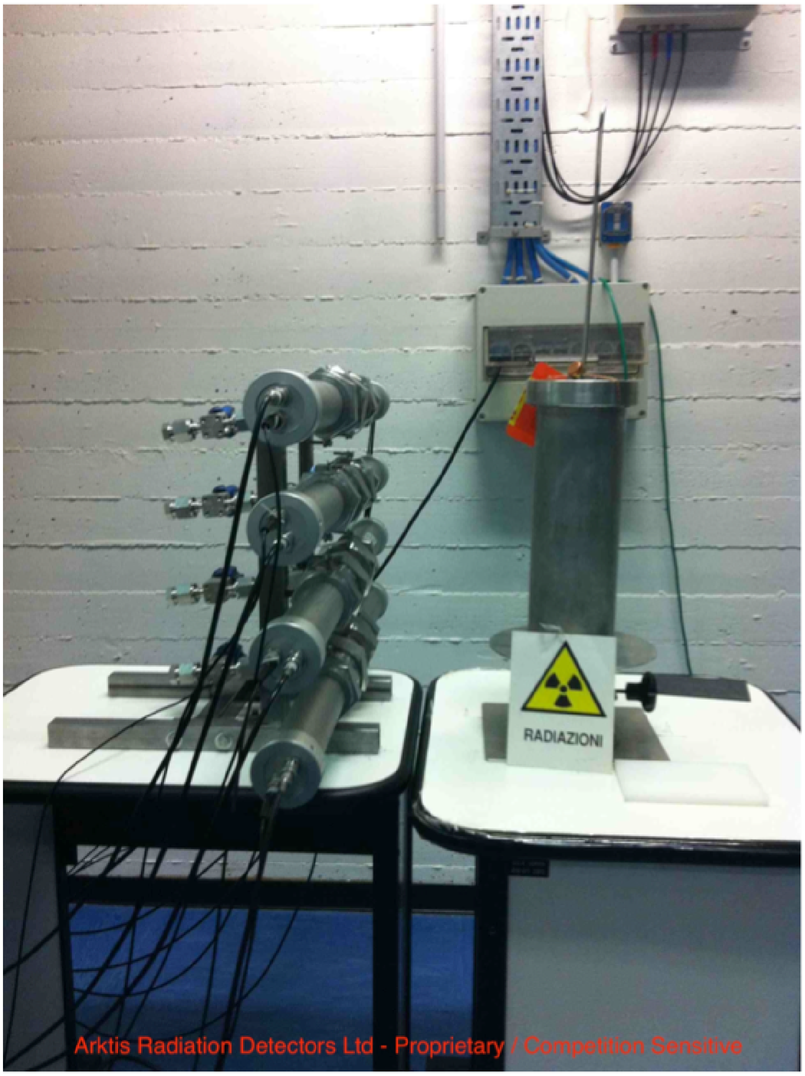

Figure 14. An array of four ^{4}He scintillation detectors used for plutonium content measurement in mixed oxide fuel.

References

[1] S. Agostinelli et al., *GEANT4 — a simulation toolkit*, *Nucl. Instrum. Meth.* **A 506** (2003) 250.

[2] J. Allison et al., *Geant4 developments and applications*, *IEEE Trans. Nucl. Sci.* **53** (2006) 270.

[3] H. Friederich et al., *A scalable DAQ system based on the DRS4 waveform digitizing chip*, *IEEE Trans. Nucl. Sci.* **58** (2011) 1652.

[4] D. Murer et al., *He-4 detectors for mixed oxide (MOX) fuel measurements*, *IEEE Nucl. Sci. Conf. R.* (2011) 4858.

[5] M.B. Chadwick et al., *ENDF/B-VII.0: next generation evaluated nuclear data library for nuclear science and technology*, *Nucl. Data Sheets* **107** (2006) 2931.

[6] S. Ritt, *Design and performance of the 6 GHz waveform digitizing chip DRS4*, *IEEE Nucl. Sci. Conf. R.* (2008) 1512.

[7] E. Aprile, A.E. Bolotnikov, A.I. Bolozdynya and T. Doke, *Scintillation detectors*, in *Noble gas detectors*, Wiley-VCH Verlag GmbH & Co. KGaA, Weinheim Germany (2006);
J.B. Birks, *The theory and practice of scintillation counting*, Pergamon Press, New York U.S.A. (1964);
G.F. Knoll, *Radiation detection and measurement*, Wiley, New York U.S.A. (1989);
B.A. Dolgosheim and B.U. Rodionov, *The mechanism of noble gas scintillation*, in *Elementary particles and cosmic rays. Volume 2*, Atomizdat, Moscow Russia (1969).

[8] D. McKinsey et al., *Time dependence of liquid helium fluorescence*, *Phys. Rev.* **A 67** (2003) 062716.